Hindawi
Journal of Mathematics
Volume 2023, Article ID 8007384, 15 pages
https://doi.org/10.1155/2023/8007384

Research Article

Numerical Method for Stochastic Nonlinear Schrödinger Equation Driven by Multivariate Gaussian Measure: Algorithms and Applications

Hongling Xie [1,2]

[1]*School of Mathematics and Statistics, Honghe University, Mengzi 661100, Yunnan, China*
[2]*School of Statistics and Mathematics, Yunnan University of Finance and Economics, Kunming 650221, Yunnan, China*

Correspondence should be addressed to Hongling Xie; xiehongling316@163.com

Received 26 February 2023; Revised 2 June 2023; Accepted 14 September 2023; Published 10 October 2023

Academic Editor: Xian-Ming Gu

In this paper, we present a novel Galerkin spectral method for numerically solving the stochastic nonlinear Schrödinger (NLS) equation driven by multivariate Gaussian random variables, including the nonlinear term. Our approach involves deriving the tensor product of triple random orthogonal basis and random functions, which enables us to effectively handle the stochasticity and nonlinear term in the equation. We apply this newly proposed method to solve both one- and two-dimensional stochastic NLS equations, providing detailed analysis and comparing the results with Monte Carlo simulation. In addition, the proposed method is applied to the stochastic Ginzburg–Landau equation. Our method exhibits excellent performance in both spatial and random spaces, achieving spectral accuracy in the numerical solutions.

1. Introduction

Nonlinear Schrödinger equation is applied in many fields of physics, such as nonlinear modulation of collisionless plasma, nonlinear wave model, nonlinear optics, and logarithmic Schrödinger equation [1–5]. In practice, some parameters in the physical equation may be uncertain or the model itself may have random disturbance and these disturbances may be related to each other. At present, the stochastic nonlinear Schrödinger equation studied are mostly driven by the Wiener process, white noise, or colored noise [6]. It has been studied theoretically and numerically and takes the form

$$id\psi + \Delta\psi \mathrm{d}t + \lambda|\psi|^2\psi \mathrm{d}t + \psi \mathrm{d}W = 0, \tag{1}$$

where $i = \sqrt{-1}$, $\lambda \in \mathbb{R}$, and W is a infinite-dimensional Wiener process.

The polarization orientation of laser plasma can be characterized by initial conditions that exhibit both randomness and interrelationships. We can use the model as follows [7]:

$$i\frac{\partial A_{\pm}(t,x)}{\partial t} + \frac{\partial^2 A_{\pm}}{\partial x^2} + \frac{2}{3}\frac{|A_{\pm}|^2 + 2|A\mp|^2}{1+\epsilon\left(|A_{\pm}|^2 + |A\mp|^2\right)}A_{\pm} = 0, \tag{2}$$

where x is the spatial variable and A_+ and A_- are the clockwise and counterclockwise circularly polarized components, respectively. The initial condition of A_+ and A_- may have the Gaussian input as

$$\begin{pmatrix} A_+ \\ A_- \end{pmatrix} = \begin{pmatrix} \alpha \\ \beta \end{pmatrix} e^{-x^2}. \tag{3}$$

The random variables α and β, which are correlated with each other, are often assumed to follow a multivariate Gaussian distribution in practical scenarios. Consequently, investigating the stochastic nonlinear Schrödinger equation driven by multivariate Gaussian random variables has become a prominent research topic. When solving this equation, the presence of the nonlinear term poses a challenging problem, regardless of whether it is driven by noise or a Gaussian random variable.

In [2], the NLS equation (1) is driven by the high-dimensional colored Wiener process. In the Hamiltonian energy space, by implementing a scalar transformation on

the noise, the uniqueness of the solution of the unknown function and the conditions for strong and weak solutions can be deduced theoretically [8]. In [3], this paper focuses on the study of the nonlinear Schrödinger equation with a point-like source term. The calculation of the nonlinear terms is closely linked to the energy norm.

In [9], the stochastic NLS equation (1) driven by white noise is numerically solved by symplectic and multisymplectic methods. The calculation of the nonlinear term in the symplectic method involves satisfying the global Lipschitz condition, while in the multisymplectic method, it is determined by ensuring the discrete charge conservation law. The two discrete schemes have good properties in long-term calculation, and both meet the discrete charge conservation principle [8, 10].

In [11], this paper presents a proof that the solution to the stochastic nonlinear Schrödinger equation can be effectively approximated by the solution of a coupled splitting scheme. Numerical calculations show that both the evolution of charge and the exponential moments of energy reach strong convergence rates. In [12], this work employs the splitting approach to approximate the NLS equation and aims at demonstrating the strong and weak order of the splitting scheme. Convergence analysis is often used in the calculation of nonlinear terms, or the stochastic value of wave function at a certain time is directly used [3].

In this paper, we consider a stochastic nonlinear Schrödinger equation driven by multivariate Gaussian random variables of the following form:

$$i\frac{\partial \psi}{\partial t} + a\Delta\psi + V(\vec{x}, \boldsymbol{\xi})\psi + \lambda|\psi|^2\psi = 0, \tag{4}$$

where $a \in \mathbb{R}$, Δ represents the Laplace operator, $V(\vec{x}, \boldsymbol{\xi})$ is some known random function, and $\vec{x}$ is the spatial vector. $\boldsymbol{\xi}$ is a multivariate Gaussian random variable.

When the higher order numerical method is required, the stochastic Galerkin (SG) spectral method is favorable [13]. The numerical calculation of the nonlinear term and how to construct orthogonal basis is a challenging problem. In previous studies, many techniques have been proposed including the probability measure transformation method [14–16], domination method [14, 17–19], measure-consistent polynomial chaos expansion method [20, 21], and Gauss–Schmidt orthogonalization method [22–28].

In [29], suppose ζ is a one-dimensional Gaussian random variable and $H(\cdot)$ represents its corresponding set of orthogonal polynomials. Let α, β, and γ be any nonnegative integer, and denote $\alpha \wedge \beta = \min\{\alpha, \beta\}$.

$$H_\alpha(\zeta)H_\beta(\zeta) = \sum_{q \le \alpha \wedge \beta} B_1(\alpha, \beta, q)H_{\alpha+\beta-2q}(\zeta), \tag{5}$$

$$\begin{aligned} B_1(\alpha, \beta, q) &= \left[\binom{\alpha}{q}\binom{\beta}{q}\binom{\alpha+\beta-2q}{\alpha-q}\right]^{1/2} \\ &= \frac{\sqrt{\alpha!\beta!(\alpha+\beta-2q)!}}{q!(\alpha-q)!(\beta-q)!}, \end{aligned} \tag{6}$$

where $\binom{\alpha}{q} = \alpha!/q!(\alpha-q)!$, and the other two parentheses of (6) do the same factorial operation. The deduced tensor product of a double orthogonal basis and random functions is applicable when $\boldsymbol{\zeta}$ is a multivariate Gaussian random variable.

Expanding on prior research, this paper aims at deducing the tensor product form of a triple random orthogonal basis (7) and random functions (8). We proposed a Galerkin spectral method for effectively solving the stochastic nonlinear Schrödinger (NLS) equation, which is driven by multivariate Gaussian random variables. In addition, we conduct numerical computations of the nonlinear term by representing it as a random function:

$$H_\alpha(\zeta)H_\beta(\zeta)H_\gamma(\zeta), \tag{7}$$

$$u(\zeta)v(\zeta)w(\zeta), \tag{8}$$

where $u(\cdot)$, $v(\cdot)$, and $w(\cdot)$ are all random functions.

Our main techniques include the following:

(i) We construct a mapping transformation that connects multivariate Gaussian random variables to independent Gaussian random variables.

(ii) Initially, we assume that the unknown function in the stochastic NLS equation can be expressed as a generalized polynomial chaos expansion. We then utilize the mapping transformation to convert it into an equation driven by independent Gaussian random variables. In addition, based on the derivations provided in Appendices A and B, we express the nonlinear term in the form of a generalized polynomial chaos expansion. Finally, we implement the stochastic Galerkin spectral method within the Gaussian measure space to solve the stochastic NLS equation.

(iii) By solving the equations derived in the process, we obtain deterministic differential equations for the coefficients of the expansion.

In addition, we employ the Monte Carlo method to simulate the stochastic NLS equation in one and two dimensions with different sample sizes. We then compare the results obtained using the proposed method with those obtained through the Monte Carlo simulation.

The organization of this paper is as follows. In Section 2, we discuss the stochastic Galerkin spectral method for solving the NLS equation driven by multivariate Gaussian measure. Section 3 presents known conclusions in the field. In Section 4, we deduce the tensor product forms of triple orthogonal basis and triple random functions. Section 5 demonstrates the application of our proposed method to solve one- and two-dimensional stochastic NLS equations. We analyze the results and compare them with those obtained using the Monte Carlo method. In addition, we apply the proposed method to the stochastic Ginzburg–Landau equation. Section 6 provides a summary of the proposed method and the results obtained.

2. Galerkin Spectral Method for the NLS Equation Driven by Multivariate Gaussian Measure

To present the method, we consider equation (4) and the unknown function $u = u(\vec{x}, \boldsymbol{\xi}(\omega))$. $\vec{x}$ is the spatial variables, and $\boldsymbol{\xi}(\omega) \in \mathbb{R}^K$ is the K-dimensional random variables with Gaussian measure. The joint probability density function is $\rho(\vec{y})$ $(\vec{y} \in \mathbb{R}^K)$, $\boldsymbol{\xi}(\boldsymbol{\omega}) = (\xi_1(\boldsymbol{\omega}), \xi_2(\boldsymbol{\omega}), \ldots, \xi_K(\boldsymbol{\omega}))$, or $\boldsymbol{\xi} = (\xi_1, \xi_2, \ldots, \xi_K)$ typically represents the uncertainties in the model.

2.1. Stochastic Galerkin Spectral Method. The procedure to design the stochastic Galerkin (SG) spectral method for (4) is as follows [19, 30, 31]:

(i) Suppose the random input function $V(\vec{x}, \boldsymbol{\xi})$, the stochastic nonlinear term $|\psi|^2$, and the unknown function $\psi(\vec{x}, t, \boldsymbol{\xi})$ have the following polynomial chaos expansion form:

$$\psi(\vec{x}, t, \boldsymbol{\xi}) \approx \psi^{N,K}(\vec{x}, t, \boldsymbol{\xi}) = \sum_{\boldsymbol{\alpha} \in \mathcal{J}^{N,K}} \widehat{\psi}_{\boldsymbol{\alpha}}(\vec{x}, t) \varphi_{\boldsymbol{\alpha}}(\boldsymbol{\xi}), \tag{9}$$

$$|\psi|^2 = \psi\overline{\psi} \approx \sum_{\boldsymbol{\alpha} \in \mathcal{J}^{N,K}} \widehat{\psi}_{\boldsymbol{\alpha}}(\vec{x}, t) \varphi_{\boldsymbol{\alpha}}(\boldsymbol{\xi}) \sum_{\boldsymbol{\beta} \in \mathcal{J}^{N,K}} \widehat{\overline{\psi}}_{\boldsymbol{\beta}}(\vec{x}, t) \varphi_{\boldsymbol{\beta}}(\boldsymbol{\xi}), \tag{10}$$

$$V(\vec{x}, \boldsymbol{\xi}) \approx V^{N,K}(\vec{x}, \boldsymbol{\xi}) = \sum_{\boldsymbol{\alpha} \in \mathcal{J}^{N,K}} \widehat{V}_{\boldsymbol{\alpha}}(\vec{x}) \varphi_{\boldsymbol{\alpha}}(\boldsymbol{\xi}), \tag{11}$$

where the orthogonal basis set $\{\varphi_{\boldsymbol{\alpha}}(\boldsymbol{\xi}), \boldsymbol{\alpha} \in \mathcal{J}^{N,K}\}$ corresponds to the dependent Gaussian variables $\boldsymbol{\xi}$. $\overline{\psi}(\cdot)$ represents its conjugate form.

(ii) Transform (4) into the equivalent variational formulation, for all orthogonal basis functions v, finding ψ such that

$$\mathbb{E}\left[i\frac{\partial \psi}{\partial t} v + a\Delta\psi(\boldsymbol{\xi}, \vec{x}) v + V(\boldsymbol{\xi}, \vec{x}) \psi(\boldsymbol{\xi}, \vec{x}) v + \lambda |\psi|^2 \psi(\boldsymbol{\xi}, \vec{x}) v \right] = 0, \tag{12}$$

where the mathematical expectation $\mathbb{E}$ is calculated according to the joint probability density function of the measure $\boldsymbol{\xi}$, and $\vec{x} \in D \subset \mathbb{R}^d$.

(iii) The weight function of v should correspond to the joint probability density function of $\boldsymbol{\xi}$ for orthogonal basis functions $v_{\mathbf{i}}$ **and** $v_{\mathbf{j}}$ satisfying the following equation for any $\{\mathbf{i}, \mathbf{j}\} \in \mathcal{J}$:

$$\int_{\Omega} v_{\mathbf{i}} v_{\mathbf{j}} \rho d\vec{y} = \begin{cases} 1, & \mathbf{i} = \mathbf{j}, \\ 0, & \mathbf{i} \neq \mathbf{j}. \end{cases} \tag{13}$$

So all of the $v = \{\varphi_{\boldsymbol{\kappa}}, \boldsymbol{\kappa} \in \mathcal{J}^{N,K}\}$, and the originally stochastic problem is reduced to the following finite-dimensional and deterministic PDE problem, for all $\varphi_{\boldsymbol{\kappa}}$, finding $\psi^{N,K}$ such that

$$\mathbb{E}\left[i\frac{\partial \psi}{\partial t} \varphi_{\boldsymbol{\kappa}} + a\Delta\psi(\vec{x}, \boldsymbol{\xi}) \varphi_{\boldsymbol{\kappa}} + V(\vec{x}, \boldsymbol{\xi}) \psi(\vec{x}, \boldsymbol{\xi}) \varphi_{\boldsymbol{\kappa}} + \lambda |\psi|^2 \psi(\vec{x}, \boldsymbol{\xi}) \varphi_{\boldsymbol{\kappa}} \right] = 0. \tag{14}$$

(iv) We use the second-order time splitting spectral method for the above deterministic problem.

We can construct the mapping relationship $\boldsymbol{\xi} \longrightarrow^T \boldsymbol{\eta}$ [31], which can potentially transform a dependent

multivariate Gaussian random vector $\boldsymbol{\xi}$ into a set of linearly independent Gaussian random variables $\boldsymbol{\eta} = (\eta_1, \eta_2, \ldots, \eta_K)$. By the maps $\mathscr{T}, \boldsymbol{\xi} = \mathscr{T}^{-1}(\boldsymbol{\eta})$, (9)–(11) and (14) can be rewritten as follows:

$$\psi^{N,K}\left(\vec{x}, t, \mathscr{T}^{-1}(\boldsymbol{\eta})\right) = \sum_{\boldsymbol{\alpha}\in\mathscr{J}^{N,K}} \widehat{\psi}_{\boldsymbol{\alpha}}(\vec{x}, t)\Phi_{\boldsymbol{\alpha}}(\boldsymbol{\eta}), \tag{15}$$

$$|\psi|^2 = \psi\overline{\psi} \approx \sum_{\boldsymbol{\alpha}\in\mathscr{J}^{N,K}} \widehat{\psi}_{\boldsymbol{\alpha}}(\vec{x}, t)\Phi_{\boldsymbol{\alpha}}(\boldsymbol{\eta}) \sum_{\boldsymbol{\beta}\in\mathscr{J}^{N,K}} \widehat{\overline{\psi}}_{\boldsymbol{\beta}}(\vec{x}, t)\Phi_{\boldsymbol{\beta}}(\boldsymbol{\eta}), \tag{16}$$

$$V^{N,K}\left(\vec{x}, \mathscr{T}^{-1}(\boldsymbol{\eta})\right) = \sum_{\boldsymbol{\alpha}\in\mathscr{J}^{N,K}} \widehat{V}_{\boldsymbol{\alpha}}(\vec{x})\Phi_{\boldsymbol{\alpha}}(\boldsymbol{\eta}), \tag{17}$$

$$\mathbb{E}\left[i\frac{\partial\psi}{\partial t}\Phi_{\boldsymbol{\beta}} + a\Delta\psi(\vec{x}, \boldsymbol{\eta})\Phi_{\boldsymbol{\beta}} + V(\vec{x}, \boldsymbol{\eta})\psi(\vec{x}, \boldsymbol{\eta})\Phi_{\boldsymbol{\beta}} + \lambda|\psi|^2\psi(\vec{x}, \boldsymbol{\eta})\Phi_{\boldsymbol{\beta}}\right] = 0. \tag{18}$$

The proposed method exhibits remarkable spectral accuracy convergence, particularly in its ability to achieve high precision in terms of the mean square error. To illustrate this concept, let us examine a scenario where both the spatial variable and the random variable are limited to a one-dimensional context. Let $u(x, t, \xi)$ and $h(x, t, \xi)$ be the exact solution and the approximate solution, respectively [30, 32].

$$\mathbb{E}\left[\|u - h\|\right]_2^2 = \sum_{j=0}^{M}\left(\int_{\Omega}\left(\widehat{u}_j(x, t) - \widehat{h}_j(x, t)\right)^2\right)\mathrm{d}x \le \frac{Q}{M^{2m-1}}t, \tag{19}$$

where Q is a constant independent of M (truncation number), t is time, and $m > 0$ is a real constant depending on the smoothness of u in terms of ξ.

3. Known Conclusion

For the random vector $\boldsymbol{\eta} = (\eta_1, \eta_2, \ldots, \eta_K)$, where $\eta_1, \eta_2, \ldots, \eta_K$ are independent to each other, by the tensor product, we may construct the multivariate polynomial as follows:

$$\Phi_{\boldsymbol{\alpha}}(\boldsymbol{\eta}) = \prod_{i=1}^{K}\phi_{\alpha_i}(\eta_i), \tag{20}$$

where $\boldsymbol{\alpha} = (\alpha_1, \ldots, \alpha_K)$ and each index $\alpha_i \in \{0, 1, 2 \ldots, N\}$. We remark that the orthogonal basis $\{\phi_n(x)\}(n = 0, 1, 2, \ldots, \infty)$ provided by (20) satisfies the orthogonality condition

$$\mathbb{E}\left(\phi_n(\eta_i)\phi_m(\eta_i)\right) = \delta_{nm} = \begin{cases} 1, & n = m, \\ 0, & n \ne m. \end{cases} \tag{21}$$

We note that $\left\{\phi_{\alpha_i}(\eta_i)\right\}_{\alpha_i=0,\ldots,N}$ is the orthogonal polynomial constructed from the Gaussian measure related to random variable η_i (see also equation (21)). Here, $\phi_{\alpha_i}(\eta_i)$ represents the Hermite polynomial.

Given a finite nonnegative integer N and K, we define a truncated multi-indicates set and some set of operations [29].

$$\mathscr{J}^{N,K} = \left\{\boldsymbol{\alpha} = (\alpha_1, \ldots, \alpha_K) \,\middle|\, \alpha_i \in \{0, \ldots, N\}, |\boldsymbol{\alpha}| = \sum_{i=1}^{K}\alpha_i \le N\right\}. \tag{22}$$

For any $\{\boldsymbol{\alpha}, \boldsymbol{\beta}, \boldsymbol{\gamma} \in \mathscr{J}\}$ and $K > 1$,

(i) **Factorial**. $\boldsymbol{\alpha}! = \prod_{i=1}^{K}\alpha_i$.

(ii) **Sizerelation**.

$$\begin{cases} \boldsymbol{\alpha}\vee\boldsymbol{\beta}: & (\max\{\alpha_i, \beta_i\}, i = 1, 2, \ldots, K), \\ \boldsymbol{\alpha}\wedge\boldsymbol{\beta}: & (\min\{\alpha_i, \beta_i\}, i = 1, 2, \ldots, K), \\ \boldsymbol{\alpha} = \boldsymbol{\beta}: & (\{\alpha_i = \beta_i\}, i = 1, 2, \ldots, K), \end{cases}$$

(iii) **AdditionSubtraction**. $\boldsymbol{\alpha} \pm \boldsymbol{\beta} = (\alpha_i \pm \beta_i, i = 1, 2, \ldots, K)$.

(iv) **Combinationfactorial**. $\binom{\boldsymbol{\alpha}}{\boldsymbol{\beta}} = \boldsymbol{\alpha}!/\boldsymbol{\beta}!(\boldsymbol{\alpha} - \boldsymbol{\beta})!$, $\binom{\boldsymbol{\alpha}}{\boldsymbol{\beta}, \boldsymbol{\gamma}} = \boldsymbol{\alpha}!/\boldsymbol{\beta}!\boldsymbol{\gamma}!(\boldsymbol{\alpha} - \boldsymbol{\beta} - \boldsymbol{\gamma})!$.

Then, any two polynomials from the set $\{\Phi_{\boldsymbol{\alpha}}(\boldsymbol{\eta}), \boldsymbol{\alpha} \in \mathscr{J}^{N,K}\}$ (here, $\{\Phi_{\boldsymbol{\alpha}}(\boldsymbol{\eta})$ is defined in (20)) are orthogonal to each other, i.e.,

$$\mathbb{E}\left[\Phi_{\boldsymbol{\alpha}}(\boldsymbol{\eta})\Phi_{\boldsymbol{\beta}}(\boldsymbol{\eta})\right] = \begin{cases} 1, & \boldsymbol{\alpha} = \boldsymbol{\beta}, \\ 0, & \boldsymbol{\alpha} \ne \boldsymbol{\beta}, \end{cases} \quad \boldsymbol{\alpha}, \boldsymbol{\beta} \in \mathscr{J}^{N,K}. \tag{23}$$

We know that the dimension number of the truncated polynomial space is

$$\dim\left\{\Phi_{\boldsymbol{\alpha}}(\boldsymbol{\eta}), \boldsymbol{\alpha} \in \mathscr{J}^{N,K}\right\} = \sum_{n=0}^{N}\binom{K + n - 1}{n} = \frac{(K + N)!}{K!N!}. \tag{24}$$

To simplify the calculation, some important conclusions of orthogonal basis are established as follows. For any $\boldsymbol{\alpha}, \boldsymbol{\beta} \in \mathscr{J}$,

$$\Phi_{\boldsymbol{\alpha}}(\boldsymbol{\eta})\Phi_{\boldsymbol{\beta}}(\boldsymbol{\eta}) = \sum_{\mathbf{q}\le\boldsymbol{\alpha}\wedge\boldsymbol{\beta}} B_1(\boldsymbol{\alpha},\boldsymbol{\beta},\mathbf{q})\Phi_{\boldsymbol{\alpha}+\boldsymbol{\beta}-2\mathbf{q}}(\boldsymbol{\eta}),$$
$$B_1(\boldsymbol{\alpha},\boldsymbol{\beta},\mathbf{q}) = \left[\binom{\boldsymbol{\alpha}}{\mathbf{q}}\binom{\boldsymbol{\beta}}{\mathbf{q}}\binom{\boldsymbol{\alpha}+\boldsymbol{\beta}-2\mathbf{q}}{\boldsymbol{\alpha}-\mathbf{q}}\right]^{1/2} = \frac{\sqrt{\boldsymbol{\alpha}!\boldsymbol{\beta}!(\boldsymbol{\alpha}+\boldsymbol{\beta}-2\mathbf{q})!}}{\mathbf{q}!(\boldsymbol{\alpha}-\mathbf{q})!(\boldsymbol{\beta}-\mathbf{q})!}, \tag{25}$$

where B_1 is similar to (6) for multi-indicates situation; for more details of (25), see [29]. Denote random functions $u = u(\vec{x}, t, \boldsymbol{\eta})$ and $v = v(\vec{x}, t, \boldsymbol{\eta})$ based on [29]

$$uv = \sum_{\boldsymbol{\theta}_1\in\mathcal{J}}\left(\sum_{\mathbf{q}\in\mathcal{J}}\sum_{0\le\boldsymbol{\beta}\le\boldsymbol{\theta}_1} C_1(\boldsymbol{\theta}_1,\boldsymbol{\beta},\mathbf{q})u_{\boldsymbol{\theta}_1-\boldsymbol{\beta}+\mathbf{q}}v_{\boldsymbol{\beta}+\mathbf{q}}\right)\Phi_{\boldsymbol{\theta}_1}(\boldsymbol{\eta}), \tag{26}$$

where $\boldsymbol{\theta}_1 = \boldsymbol{\alpha}+\boldsymbol{\beta}$, $\mathbf{q}\le\boldsymbol{\alpha}\wedge\boldsymbol{\beta}$, and

$$C_1(\boldsymbol{\theta}_1,\boldsymbol{\beta},\mathbf{q}) = \left[\binom{\boldsymbol{\theta}_1}{\boldsymbol{\beta}}\binom{\boldsymbol{\beta}+\mathbf{q}}{\mathbf{q}}\binom{\boldsymbol{\theta}_1-\boldsymbol{\beta}+\mathbf{q}}{\mathbf{q}}\right]^{1/2} = \frac{\sqrt{\boldsymbol{\theta}_1!(\boldsymbol{\beta}+\mathbf{q})!(\boldsymbol{\theta}_1-\boldsymbol{\beta}+\mathbf{q})!}}{\mathbf{q}!\boldsymbol{\beta}!(\boldsymbol{\theta}_1-\boldsymbol{\beta})!}. \tag{27}$$

4. Tensor Product of Triple Random Orthogonal Basis and Random Functions

In this section, we deduced the tensor product of a triple random orthogonal basis and random functions by relying on established conclusions.

$$\phi_\alpha(\eta)\phi_\beta(\eta)\phi_\gamma(\eta) = \sum_{p\le\alpha\wedge\gamma}\sum_{q\le\alpha\wedge\beta}\sum_{r\le\beta\wedge\gamma} B_2(\alpha,\beta,\gamma,p,q,r)\phi_{\alpha+\beta+\gamma-2(p+q+r)}(\eta), \tag{28}$$

$$B_2(\alpha,\beta,\gamma,p,q,r) = \left[\binom{\alpha}{p,q}\binom{\beta}{q,r}\binom{\gamma}{p,r}\binom{\alpha+\beta+\gamma-2(p+q+r)}{\alpha-p-q,\beta-q-r}\right]^{1/2} = \frac{\sqrt{\alpha!\beta!\gamma!}\sqrt{\alpha+\beta+\gamma-2(p+q+r)}}{p!q!r!(\alpha-p-q)!(\beta-q-r)!(\gamma-p-r)!}. \tag{29}$$

In combination with Appendix A, for any $\boldsymbol{\alpha},\boldsymbol{\beta},\boldsymbol{\gamma}\in\mathcal{J}^{N,K}$, we have a multi-indicates situation as follows:

$$B_2(\boldsymbol{\alpha},\boldsymbol{\beta},\boldsymbol{\gamma},\mathbf{p},\mathbf{q},\mathbf{r}) = \left[\binom{\boldsymbol{\alpha}}{\mathbf{p},\mathbf{q}}\binom{\boldsymbol{\beta}}{\mathbf{q},\mathbf{r}}\binom{\boldsymbol{\gamma}}{\mathbf{p},\mathbf{r}}\binom{\boldsymbol{\alpha}+\boldsymbol{\beta}+\boldsymbol{\gamma}-2(\mathbf{p}+\mathbf{q}+\mathbf{r})}{\boldsymbol{\alpha}-\mathbf{p}-\mathbf{q},\boldsymbol{\beta}-\mathbf{q}-\mathbf{r}}\right]^{1/2},$$
$$\Phi_{\boldsymbol{\alpha}}\Phi_{\boldsymbol{\beta}}\Phi_{\boldsymbol{\gamma}} = \sum_{\mathbf{p}\le\boldsymbol{\alpha}\wedge\boldsymbol{\gamma}}\sum_{\mathbf{q}\le\boldsymbol{\alpha}\wedge\boldsymbol{\beta}}\sum_{\mathbf{r}\le\boldsymbol{\beta}\wedge\boldsymbol{\gamma}} B_2(\boldsymbol{\alpha},\boldsymbol{\beta},\boldsymbol{\gamma},\mathbf{p},\mathbf{q},\mathbf{r})\Phi_{\boldsymbol{\alpha}+\boldsymbol{\beta}+\boldsymbol{\gamma}-2(\mathbf{p}+\mathbf{q}+\mathbf{r})}(\boldsymbol{\eta}). \tag{30}$$

The proof of (28) and (29) can be seen in Appendix A.

Through our numerical calculations, we have derived the following conclusions pertaining to the triple random unknown function. Suppose u, v, and w have the following SG chaos expansion:

$$\begin{aligned} u^{N,K}\left(\vec{x},t,\mathscr{T}^{-1}(\boldsymbol{\eta})\right) &= \sum_{\boldsymbol{\alpha}\in\mathscr{J}^{N,K}} \widehat{u}_{\boldsymbol{\alpha}}(\vec{x},t)\Phi_{\boldsymbol{\alpha}}(\boldsymbol{\eta}),\\ v^{N,K}\left(\vec{x},t,\mathscr{T}^{-1}(\boldsymbol{\eta})\right) &= \sum_{\boldsymbol{\beta}\in\mathscr{J}^{N,K}} \widehat{v}_{\boldsymbol{\beta}}(\vec{x},t)\Phi_{\boldsymbol{\beta}}(\boldsymbol{\eta}),\\ w^{N,K}\left(\vec{x},t,\mathscr{T}^{-1}(\boldsymbol{\eta})\right) &= \sum_{\boldsymbol{\gamma}\in\mathscr{J}^{N,K}} \widehat{w}_{\boldsymbol{\gamma}}(\vec{x},t)\Phi_{\boldsymbol{\gamma}}(\boldsymbol{\eta}). \end{aligned} \tag{31}$$

In combination with Appendix B, we have the following multi-indicates situation:

$$\begin{aligned} uvw &= \sum_{\boldsymbol{\theta}_2\in\mathscr{J}} \widehat{uvw}_{\boldsymbol{\theta}_2}\Phi_{\boldsymbol{\theta}_2}(\boldsymbol{\eta}),\\ \widehat{uvw}_{\boldsymbol{\theta}_2} &= \sum_{\mathbf{p}\in\mathscr{J}}\sum_{\mathbf{q}\in\mathscr{J}}\sum_{\mathbf{r}\in\mathscr{J}}\sum_{\boldsymbol{\theta}_2=\boldsymbol{\alpha}+\boldsymbol{\beta}+\boldsymbol{\gamma}} C_2(\mathbf{p},\mathbf{q},\mathbf{r},\boldsymbol{\theta}_2,\boldsymbol{\alpha},\boldsymbol{\beta},\boldsymbol{\gamma})u_{\boldsymbol{\alpha}+\mathbf{p}+\mathbf{q}}v_{\boldsymbol{\beta}+\mathbf{q}+\mathbf{r}}w_{\boldsymbol{\gamma}+\mathbf{r}+\mathbf{p}}, \end{aligned} \tag{32}$$

where $\boldsymbol{\theta}_2 = \boldsymbol{\alpha}+\boldsymbol{\beta}+\boldsymbol{\gamma}$, $\mathbf{p}\le\boldsymbol{\alpha}\wedge\boldsymbol{\gamma}$, $\mathbf{q}\le\boldsymbol{\alpha}\wedge\boldsymbol{\beta}$, $\mathbf{r}\le\boldsymbol{\beta}\wedge\boldsymbol{\gamma}$, and the multi-indicates situation

$$\begin{aligned} C_2(\boldsymbol{\theta}_2,\mathbf{p},\mathbf{q},\mathbf{r},\boldsymbol{\alpha},\boldsymbol{\beta},\boldsymbol{\gamma}) &= \left[\binom{\boldsymbol{\theta}_2}{\boldsymbol{\alpha},\boldsymbol{\beta}}\binom{\boldsymbol{\alpha}+\mathbf{p}+\mathbf{q}}{\mathbf{p},\mathbf{q}}\binom{\boldsymbol{\beta}+\mathbf{q}+\mathbf{r}}{\mathbf{q},\mathbf{r}}\binom{\boldsymbol{\gamma}+\mathbf{p}+\mathbf{r}}{\mathbf{p},\mathbf{r}}\right]^{1/2}\\ &= \frac{\sqrt{(\boldsymbol{\alpha}+\mathbf{p}+\mathbf{q})!(\boldsymbol{\beta}+\mathbf{q}+\mathbf{r})!(\boldsymbol{\gamma}+\mathbf{p}+\mathbf{r})!\boldsymbol{\theta}_2!}}{\mathbf{p}!\mathbf{q}!\mathbf{r}!\boldsymbol{\alpha}!\boldsymbol{\beta}!\boldsymbol{\gamma}!}. \end{aligned} \tag{33}$$

The proof of (32) and (33) can be seen in Appendix B.

5. Numerical Experiments

In this section, we test the accuracy of the proposed method by solving stochastic one- and two-dimensional NLS equations, respectively. All the presented stochastic equations are driven by bivariate random Gaussian variables. In addition, we assume that the unknown function have a periodic boundary condition in the spatial direction and will use the Fourier spectral method to approximate the unknown function ψ [33, 34].

To minimize computational costs, we can derive the conclusions by utilizing equations (26) and (32), which are obtained from the application of equations (15)–(17).

$$\begin{aligned} \psi V \approx \psi^{N,K}V^{N,K} &= \sum_{\boldsymbol{\alpha}\in\mathscr{J}^{N,K}} \widehat{\psi}_{\boldsymbol{\alpha}}(\vec{x},t)\Phi_{\boldsymbol{\alpha}}(\boldsymbol{\eta}) \sum_{\boldsymbol{\beta}\in\mathscr{J}^{N,K}} \widehat{V}_{\boldsymbol{\beta}}(\vec{x},t)\Phi_{\boldsymbol{\beta}}(\boldsymbol{\eta})\\ &= \sum_{\boldsymbol{\theta}_1\in\mathscr{J}}\left(\sum_{\mathbf{q}\in\mathscr{J}}\sum_{\mathbf{0}\le\boldsymbol{\beta}\le\boldsymbol{\theta}_1} C_1(\boldsymbol{\theta}_1,\boldsymbol{\beta},\mathbf{q})\widehat{\psi}_{\boldsymbol{\theta}_1-\boldsymbol{\beta}+\mathbf{q}}\widehat{V}_{\boldsymbol{\beta}+\mathbf{q}}\right)\Phi_{\boldsymbol{\theta}_1}(\boldsymbol{\eta}),\\ |\psi|^2\psi = \psi\psi\overline{\psi} \approx \sum_{\boldsymbol{\alpha}\in\mathscr{J}^{N,K}} \widehat{\psi}_{\boldsymbol{\alpha}}(\vec{x},t)\Phi_{\boldsymbol{\alpha}}(\boldsymbol{\eta}) \sum_{\boldsymbol{\beta}\in\mathscr{J}^{N,K}} \widehat{\psi}_{\boldsymbol{\beta}}(\vec{x},t)\Phi_{\boldsymbol{\beta}}(\boldsymbol{\eta}) \sum_{\boldsymbol{\gamma}\in\mathscr{J}^{N,K}} \widehat{\overline{\psi}}_{\boldsymbol{\gamma}}(\vec{x},t)\Phi_{\boldsymbol{\gamma}}(\boldsymbol{\eta}) &= \sum_{\boldsymbol{\theta}_2\in\mathscr{J}} \Gamma_{\boldsymbol{\theta}_2}\Phi_{\boldsymbol{\theta}_2}(\boldsymbol{\eta}),\\ \Gamma_{\boldsymbol{\theta}_2} = \sum_{\mathbf{p}\in\mathscr{J}}\sum_{\mathbf{q}\in\mathscr{J}}\sum_{\mathbf{r}\in\mathscr{J}}\sum_{\boldsymbol{\theta}_2=\boldsymbol{\alpha}+\boldsymbol{\beta}+\boldsymbol{\gamma}} C_2(\mathbf{p},\mathbf{q},\mathbf{r},\boldsymbol{\theta}_2,\boldsymbol{\alpha},\boldsymbol{\beta},\boldsymbol{\gamma})\widehat{\psi}_{\boldsymbol{\alpha}+\mathbf{p}+\mathbf{q}}\widehat{\psi}_{\boldsymbol{\beta}+\mathbf{q}+\mathbf{r}}\widehat{\overline{\psi}}_{\boldsymbol{\gamma}+\mathbf{r}+\mathbf{p}}. \end{aligned} \tag{34}$$

Then, (18) is equivalent to the Galerkin system as follows:

$$i(\widehat{\psi}_{\boldsymbol{\kappa}})_t + a\Delta\widehat{\psi}_{\boldsymbol{\kappa}} + \sum_{\mathbf{q}\in\mathscr{J}}\sum_{\mathbf{0}\le\boldsymbol{\beta}\le\boldsymbol{\kappa}} C_1(\boldsymbol{\kappa},\boldsymbol{\beta},\mathbf{q})\widehat{\psi}_{\boldsymbol{\kappa}-\boldsymbol{\beta}+\mathbf{q}}\widehat{V}_{\boldsymbol{\beta}+\mathbf{q}} + \lambda\sum_{\mathbf{p}\in\mathscr{J}}\sum_{\mathbf{q}\in\mathscr{J}}\sum_{\mathbf{r}\in\mathscr{J}}\sum_{\boldsymbol{\kappa}=\boldsymbol{\alpha}+\boldsymbol{\beta}+\boldsymbol{\gamma}} C_2(\mathbf{p},\mathbf{q},\mathbf{r},\boldsymbol{\kappa},\boldsymbol{\alpha},\boldsymbol{\beta},\boldsymbol{\gamma})\widehat{\psi}_{\boldsymbol{\alpha}+\mathbf{p}+\mathbf{q}}\widehat{\psi}_{\boldsymbol{\beta}+\mathbf{q}+\mathbf{r}}\widehat{\overline{\psi}}_{\boldsymbol{\gamma}+\mathbf{r}+\mathbf{p}} = 0. \tag{35}$$

To solve the Galerkin system (35) numerically, in the spatial and time direction of the Galerkin system, we used the Fourier spectral method and the second-order time splitting method, respectively. We used the pseudospectral method to compute the Fourier coefficients of $\widehat{\psi}_{\boldsymbol{\kappa}-\boldsymbol{\beta}+\mathbf{q}}\widehat{V}_{\boldsymbol{\beta}+\mathbf{q}}$ and $\widehat{\psi}_{\boldsymbol{\alpha}+\mathbf{p}+\mathbf{q}}\widehat{\psi}_{\boldsymbol{\beta}+\mathbf{q}+\mathbf{r}}\widehat{\overline{\psi}}_{\boldsymbol{\gamma}+\mathbf{r}+\mathbf{p}}$ [29]. The expectation, second-order moment, and variance of $\psi(\vec{x},t)$ can be calculated as follows:

$$\begin{aligned}\mathbb{E}[\psi(\vec{x},t)] &= \widehat{\psi}_{\mathbf{0}},\\ \mathbb{E}\left[\psi^2(\vec{x},t)\right] &= \sum_{\boldsymbol{\alpha}\in\mathscr{J}^{N,K}}\widehat{\psi}_{\boldsymbol{\alpha}}^2,\\ \mathrm{Var}[\psi(\vec{x},t)] &= \sum_{\boldsymbol{\alpha}\in\mathscr{J}^{N,K}}\widehat{\psi}_{\boldsymbol{\alpha}}^2 - \widehat{\psi}_{\mathbf{0}}^2.\end{aligned} \tag{36}$$

To demonstrate the accuracy of this method, we define the errors in terms of expectation and variance for the real and imaginary parts, respectively.

$$\begin{aligned}\mathbb{E}_{\mathrm{error}}^{\mathrm{real}} &= \left|\mathrm{real}\left[\mathbb{E}\left[\psi^{N,K}\right] - \mathbb{E}\left[\psi_{\mathrm{exact}}\right]\right]\right|_{\max},\\ \mathbb{E}_{\mathrm{error}}^{\mathrm{imag}} &= \left|\mathrm{imag}\left[\mathbb{E}\left[\psi^{N,K}\right] - \mathbb{E}\left[\psi_{\mathrm{exact}}\right]\right]\right|_{\max},\\ \mathrm{Var}_{\mathrm{error}}^{\mathrm{real}} &= \left|\mathrm{real}\left[\mathrm{Var}\left[\psi^{N,K}\right] - \mathrm{Var}\left[\psi_{\mathrm{exact}}\right]\right]\right|_{\max},\\ \mathrm{Var}_{\mathrm{error}}^{\mathrm{imag}} &= \left|\mathrm{imag}\left[\mathrm{Var}\left[\psi^{N,K}\right] - \mathrm{Var}\left[\psi_{\mathrm{exact}}\right]\right]\right|_{\max},\end{aligned} \tag{37}$$

where $|\cdot|$, real$[\cdot]$, and imag$[\cdot]$ represent the absolute value, real part, and imaginary part, respectively. The errors $\mathbb{E}_{\mathrm{error}}^{[\cdot]}$ and $\mathrm{Var}_{\mathrm{error}}^{[\cdot]}$ correspond to the deviations in the real and imaginary parts of the expectation and variance, respectively. To emphasize the accuracy and efficiency of the proposed method, we employ the Monte Carlo method to simulate the stochastic NLS equations in one and two dimensions using varying sample sizes. A comparative analysis is then performed between the Monte Carlo method and the proposed method.

5.1. Stochastic 1D NLS Equation. Consider the following stochastic one-dimensional NLS equation:

$$i\frac{\partial\psi}{\partial t} + a\frac{\partial^2\psi}{\partial x^2} + V(x,\boldsymbol{\xi})\psi + \lambda|\psi|^2\psi = 0, \quad x\in[-6\pi,6\pi], \tag{38}$$

where $\vec{x} = x$.

$$\begin{aligned}\psi_0 &= f(\boldsymbol{\xi})\sin(x),\\ V(x,\boldsymbol{\xi}) &= f(\boldsymbol{\xi})^2\sin^2(x) - b,\\ f(\boldsymbol{\xi}) &= 1 + \sqrt{2}\left[\frac{1}{\sqrt{1.9}}(\xi_1+\xi_2) - \sqrt{10}(\xi_1-\xi_2)\right],\\ \lambda &= -1, a = 1, b = 1.\end{aligned} \tag{39}$$

Equation (38) has the following analytical solution:

$$\psi_{\mathrm{exact}} = f(\xi_1,\xi_2)e^{-2it}\sin(x). \tag{40}$$

The random variables $\boldsymbol{\xi} = (\xi_1,\xi_2) \sim N(\mu_1,\mu_2,\sigma_1^2,\sigma_2^2,R)$ (i.e., they are bivariate Gaussian random variables). $\mu_1,\mu_2,\sigma_1^2,\sigma_2^2,$ and R are some known constants ($\mu_1 = \mu_2 = 0, \sigma_1^2 = \sigma_2^2 = 0.25, R = 0.9$ is taken in our calculation later).

Based on the maps $\mathscr{T}$ between $\boldsymbol{\xi}$ and $\boldsymbol{\eta}$,

$$\begin{aligned}\xi_1 &= -\frac{\sqrt{2}}{2}\left(\sqrt{0.025}\,\eta_1 - \sqrt{0.475}\,\eta_2\right),\\ \xi_2 &= \frac{\sqrt{2}}{2}\left(\sqrt{0.025}\,\eta_1 + \sqrt{0.475}\,\eta_2\right).\end{aligned} \tag{41}$$

Then, $f(\boldsymbol{\xi})$ and $V(x,\boldsymbol{\xi})$ can be rewritten as follows:

$$\begin{aligned}f(\xi_1,\xi_2) &= 1 + \eta_1 + \eta_2,\\ V(x,\xi_1,\xi_2) &= (1+\eta_1+\eta_2)^2\sin^2(x) - b.\end{aligned} \tag{42}$$

In Example 1, Tables 1–4 present a summary of our results, illustrating the errors in the real and imaginary parts of the expectation and variance of the random solution at different time points. On the other hand, Tables 5–8 display the results obtained through Monte Carlo simulations for equation (38).

Figure 1(a) displays the real and imaginary components of the expectation of the approximation solution. Figure 1(b) depicts the real and imaginary parts of the error in the expectation (top) and variance (bottom) for equation (38) at $T = 2$.

5.2. Stochastic 2D NLS Equation. Consider the following stochastic two-dimensional NLS equation with the same random function $f(\boldsymbol{\xi})$ as one-dimensional case:

Table 1: The real part of the expectation error for the solution equation (38) at different time points by the proposed method and with time step $\Delta t = 0.0001$.

t	$t = 0.3$	$t = 0.5$	$t = 0.8$	$t = 1$	$t = 1.5$
$\mathbb{E}_{\text{error}}^{\text{real}}$	$1.09474E-4$	$3.9075E-5$	$1.5473E-4$	$2.3408E-4$	$1.3733E-4$

Table 2: The imaginary part of expectation error for the solution equation (38) at different time points by the proposed method and with time step $\Delta t = 0.0001$.

t	$t = 0.3$	$t = 0.5$	$t = 0.8$	$t = 1$	$t = 1.5$
$\mathbb{E}_{\text{error}}^{\text{imag}}$	$1.3834E-4$	$4.9246E-5$	$3.0282E-5$	$6.1699E-5$	$5.2435E-4$

Table 3: The real part of the variance error for the solution equation (38) at different time points by the proposed method and with time step $\Delta t = 0.0001$.

t	$t = 0.3$	$t = 0.5$	$t = 0.8$	$t = 1$	$t = 1.5$
$\text{Var}_{\text{error}}^{\text{real}}$	$6.2920E-4$	$3.3184E-4$	$8.0057E-5$	$8.7284E-4$	$1E-3$

Table 4: The imaginary part of the variance error for the solution equation (38) at different time points by the proposed method and with time step $\Delta t = 0.0001$.

t	$t = 0.3$	$t = 0.5$	$t = 0.8$	$t = 1$	$t = 1.5$
$\text{Var}_{\text{error}}^{\text{imag}}$	$1.9928E-4$	$7.0690E-5$	$8.4386E-4$	$9.5322E-4$	$2.7E-3$

Table 5: The real part of the expectation error for the solution equation (38) for different sample sizes and different time points by Monte Carlo simulation and with time step $\Delta t = 0.01$.

t	$t = 0.3$	$t = 0.5$	$t = 0.8$	$t = 1$	$t = 1.5$	
$\mathbb{E}_{\text{error}}^{\text{real}}$	0.0091	0.0058	$1.5581E-4$	0.0028	0.0135	$\mathcal{S} = 10^4$
$\mathbb{E}_{\text{error}}^{\text{real}}$	0.0011	0.0021	$7.6401E-5$	$7.1761E-4$	0.0055	$\mathcal{S} = 10^5$

$\mathcal{S}$ represents the sample size.

Table 6: The imaginary part of expectation error for the solution equation (38) for different sample sizes and different time points by Monte Carlo simulation and with time step $\Delta t = 0.01$.

t	$t = 0.3$	$t = 0.5$	$t = 0.8$	$t = 1$	$t = 1.5$	
$\mathbb{E}_{\text{error}}^{\text{imag}}$	0.0062	0.009	0.0053	0.0061	0.0019	$\mathcal{S} = 10^4$
$\mathbb{E}_{\text{error}}^{\text{imag}}$	$7.3979E-4$	0.0032	0.0026	0.0016	$7.8633E-4$	$\mathcal{S} = 10^5$

$\mathcal{S}$ represents the sample size.

Table 7: The real part of the variance error for the solution equation (38) for different sample sizes and different time points by Monte Carlo simulation and with time step $\Delta t = 0.01$.

t	$t = 0.3$	$t = 0.5$	$t = 0.8$	$t = 1$	$t = 1.5$	
$\text{Var}_{\text{error}}^{\text{real}}$	0.0048	0.0066	0.0078	0.0232	0.0369	$\mathcal{S} = 10^4$
$\text{Var}_{\text{error}}^{\text{real}}$	$1.8037E-4$	0.0078	$7.372E-4$	0.0029	0.007	$\mathcal{S} = 10^5$

$\mathcal{S}$ represents the ample size.

Table 8: The imaginary part of the variance error for the solution equation (38) for different sample sizes and different time points by Monte Carlo simulation and with time step $\Delta t = 0.01$.

t	$t = 0.3$	$t = 0.5$	$t = 0.8$	$t = 1$	$t = 1.5$	
$\text{Var}_{\text{error}}^{\text{imag}}$	0.0124	0.0144	$4.5566E-4$	0.0269	0.0108	$\mathcal{S} = 10^4$
$\text{Var}_{\text{error}}^{\text{imag}}$	$4.6393E-4$	0.017	$4.3107E-5$	0.0034	0.002	$\mathcal{S} = 10^5$

$\mathcal{S}$ represents the sample size.

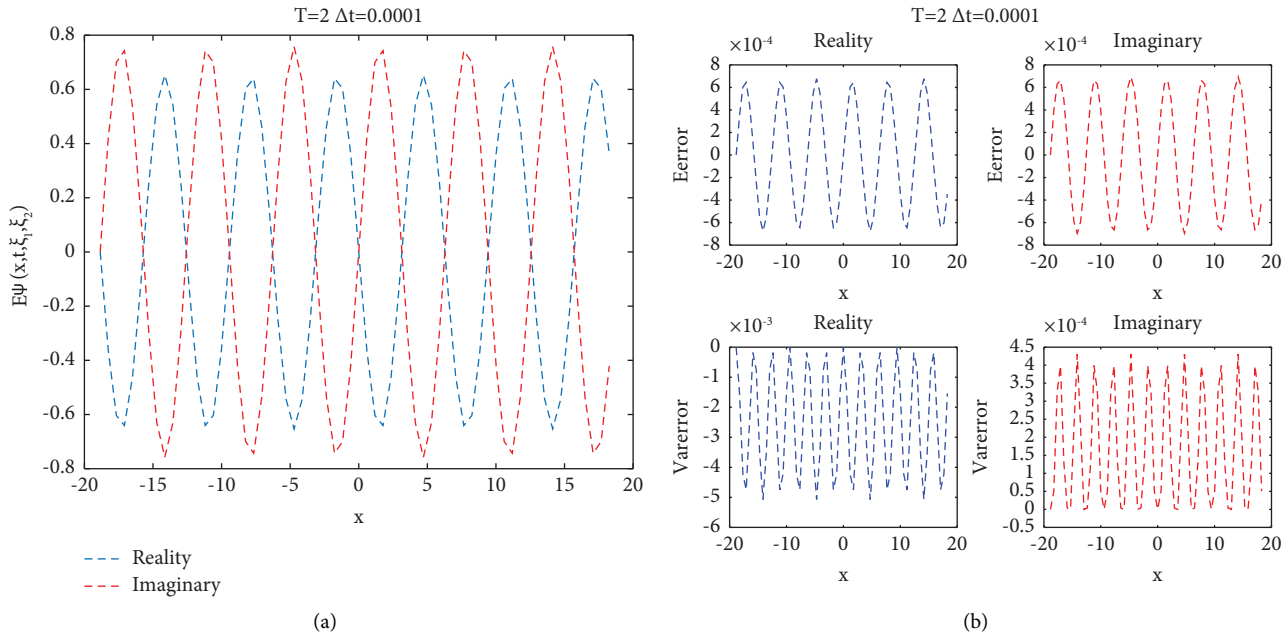

FIGURE 1: (a) Plots of the expectation of approximation solution for equation (38) at $T = 2$. The red and blue dashed lines represent the real and imaginary parts of the approximate solution, respectively. (b) Plots of the real and imaginary parts of the errors in the expectation (top) and variance (bottom), respectively. The time step is $\Delta t = 0.0001$.

TABLE 9: The real part of expectation error for the solution equation (43) at different time points by the proposed method and with time step $\Delta t = 0.000001$.

t	$t = 0.3$	$t = 0.5$	$t = 0.8$	$t = 1$	$t = 1.5$
$\mathbb{E}_{\text{error}}^{\text{real}}$	$9.769E-8$	$9.9034E-7$	$5.0436E-6$	$1.013E-5$	$1.6847E-5$

$$i\frac{\partial \psi}{\partial t} + 0.5a\left(\frac{\partial^2 \psi}{\partial x^2} + \frac{\partial^2 \psi}{\partial y^2}\right) + V(x, y, \boldsymbol{\xi})\psi + \lambda|\psi|^2\psi = 0, \tag{43}$$

where $\overrightarrow{x} = (x, y)$, $(x, y) \in [-6\pi, 6\pi] \times [-6\pi, 6\pi]$.

$$\begin{aligned} \psi_0 &= f(\boldsymbol{\xi}) \sin(x) \sin(y), \\ V(x, y, \boldsymbol{\xi}) &= f(\boldsymbol{\xi})^2 sin^2(x) \sin^2(y) - b, \\ \lambda &= -1, a = 1, b = 1. \end{aligned} \tag{44}$$

Equation (43) has the following analytical solution:

$$\psi_{\text{exact}} = f(\xi_1, \xi_2) e^{-2it} \sin(x) \sin(y). \tag{45}$$

In Example 2, we present the summary of our results in Tables 9–12, which demonstrate the errors in the real and imaginary parts of the expectation and variance of the random solution at different time points. In addition, Tables 13–16 display the results obtained through Monte Carlo simulations for equation (43).

Figure 2(a) illustrates the real and imaginary components of the expectation of the approximation solution. Figure 2(b) presents the real and imaginary parts of the error in the expectation (top) and variance (bottom) for equation (43) at $T = 2$, respectively.

By analyzing the data presented in Tables 1–4 and 9–12, along with Figures 1 and 2, it becomes evident that the proposed method achieves spectral accuracy in the context of the stochastic nonlinear Schrödinger equation with multivariate Gaussian measure, even in long-time scenarios. In comparison, Tables 5–8 and 13–16 indicate that Monte Carlo simulation does not exhibit high accuracy. Even when the accuracy occasionally reaches spectral accuracy, the computational cost remains significant and the overall efficiency is low.

5.3. Application. This section discussed the application of stochastic Ginzburg–Landau equation of the following forms:

$$\frac{\partial u}{\partial t} + \frac{i}{2}(\beta + ig\tau)\frac{\partial^2 u}{\partial x^2} + i\gamma|u|^2 u + \frac{1}{2}gu = -\frac{1}{2}\alpha u, \tag{46}$$

where $\tau = 0.01, \beta = -1, g = -1$. The initial condition is

$$u_0(t, x, \xi_1, \xi_2) = \text{sech}(\xi_1 x) e^{i\xi_2 x}. \tag{47}$$

The distribution of random variables $(\xi_1, \xi_2) \sim N(\mu_1, \mu_2, \sigma_1^2, \sigma_2^2, R)$ is the same as Example 1. For $\gamma = 0.1$, we use $\alpha = 0.01$, $\alpha = 1$, $\alpha = 1.2$, and $\alpha = 3$.

Table 10: The imaginary part of expectation error for the solution equation (43) at different time points by the proposed method and with time step $\Delta t = 0.000001$.

t	$t = 0.3$	$t = 0.5$	$t = 0.8$	$t = 1$	$t = 1.5$
$\mathbb{E}_{\text{error}}^{\text{imag}}$	$4.2669E-7$	$1.0061E-6$	$6.2788E-7$	$3.0115E-6$	$5.8374E-5$

Table 11: The real part of the variance error for the solution equation (43) at different time points by the proposed method and with time step $\Delta t = 0.000001$.

t	$t = 0.3$	$t = 0.5$	$t = 0.8$	$t = 1$	$t = 1.5$
$\text{Var}_{\text{error}}^{\text{real}}$	$2.3195E-5$	$4.4213E-5$	$4.1201E-6$	$9.7694E-5$	$1.989E-4$

Table 12: The imaginary part of the variance error for the solution equation (43) at different time points by the proposed method and with time step $\Delta t = 0.000001$.

t	$t = 0.3$	$t = 0.5$	$t = 0.8$	$t = 1$	$t = 1.5$
$\text{Var}_{\text{error}}^{\text{imag}}$	$1.0554E-5$	$1.634E-5$	$9.4247E-5$	$1.0701E-4$	$4.3271E-4$

Table 13: The real part of expectation error for the solution equation (43) for different sample sizes and different time points by Monte Carlo simulation and with time step $\Delta t = 0.01$.

t	$t = 0.3$	$t = 0.5$	$t = 0.8$	$t = 1$	$t = 1.5$	
$\mathbb{E}_{\text{error}}^{\text{real}}$	$2.8411E-4$	0.0021	$5.3607E-4$	$7.0779E-4$	0.0127	$\mathcal{S} = 10^4$
$\mathbb{E}_{\text{error}}^{\text{real}}$	$6.9489E-4$	$3.3865E-4$	$2.4584E-5$	$2.6083E-4$	0.0042	$\mathcal{S} = 10^5$

$\mathcal{S}$ represents the sample size.

Table 14: The imaginary part of the expectation error for the solution equation (43) for different sample sizes and different time points by Monte Carlo simulation and with time step $\Delta t = 0.01$.

t	$t = 0.3$	$t = 0.5$	$t = 0.8$	$t = 1$	$t = 1.5$	
$\mathbb{E}_{\text{error}}^{\text{imag}}$	$1.9437E-4$	0.0032	0.0184	0.0015	0.0018	$\mathcal{S} = 10^4$
$\mathbb{E}_{\text{error}}^{\text{imag}}$	$4.754E-4$	$5.2741E-4$	$8.4158E-4$	$5.6993E-4$	$5.9161E-4$	$\mathcal{S} = 10^5$

$\mathcal{S}$ represents the sample size.

Table 15: The real part of the variance error for the solution equation (43) for different sample sizes and different time points by Monte Carlo simulation and with time step $\Delta t = 0.01$.

t	$t = 0.3$	$t = 0.5$	$t = 0.8$	$t = 1$	$t = 1.5$	
$\text{Var}_{\text{error}}^{\text{real}}$	0.0089	0.0189	0.0261	0.0375	$3.3E-3$	$\mathcal{S} = 10^4$
$\text{Var}_{\text{error}}^{\text{real}}$	0.0026	0.0016	0.0073	0.0025	$9.3E-3$	$\mathcal{S} = 10^5$

$\mathcal{S}$ represents the sample size.

Table 16: The imaginary part of the variance error for the solution equation (43) for different sample sizes and different time points by Monte Carlo simulation and with time step $\Delta t = 0.01$.

t	$t = 0.3$	$t = 0.5$	$t = 0.8$	$t = 1$	$t = 1.5$	
$\text{Var}_{\text{error}}^{\text{imag}}$	0.0228	0.0414	0.0015	0.0435	$9.5616E-4$	$\mathcal{S} = 10^4$
$\text{Var}_{\text{error}}^{\text{imag}}$	0.0068	0.0034	$4.2521E-4$	0.0029	0.0027	$\mathcal{S} = 10^5$

$\mathcal{S}$ represents the sample size.

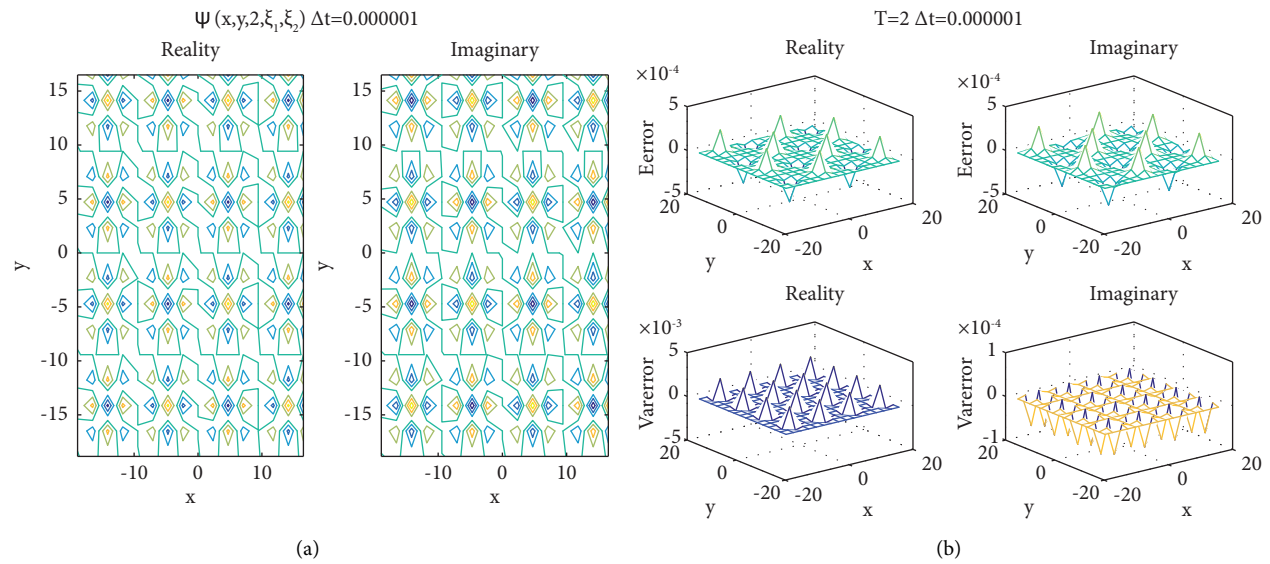

FIGURE 2: (a) Plots of the expectation of approximation solution for equation (43) at $T = 2$. (b) Plots of the real and imaginary parts of the errors in the expectation (top) and variance (bottom), respectively. The time step is $\Delta t = 0.000001$.

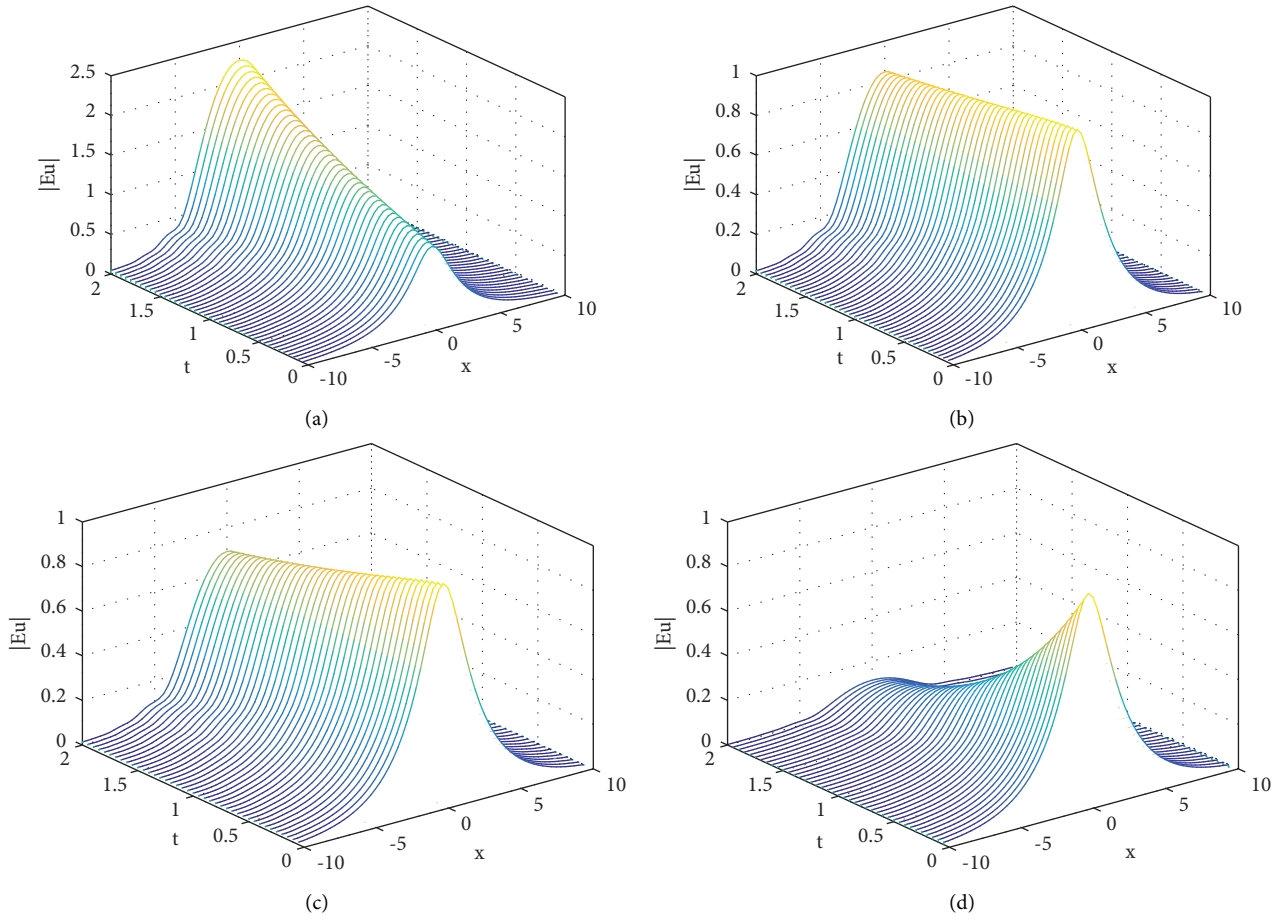

FIGURE 3: The expectation of amplitude of approximation solution for equation (46) at different time points for different parameters. The time step is $\Delta t = 0.001$. (a–d) Corresponding to the cases where $\alpha = 0.01, 0.1, 1.2,$ and 3, respectively.

In Figure 3, we present the expectation of the amplitude of the approximation solution for equation (46) at various time points, considering different parameter values. Specifically, Figures 3(a)–3(d) correspond to the cases where α takes the values of 0.01, 0.1, 1.2, and 3, respectively.

6. Concluding Remarks

We have developed a novel spectral numerical method for solving the stochastic nonlinear Schrödinger equation driven by multivariate Gaussian measure. This method demonstrates spectral accuracy in both spatial and random spaces, even in long-term scenarios. We applied this efficient and accurate numerical method to investigate the one- and two-dimensional stochastic NLS equations driven by bivariate Gaussian variables. In order to compare the accuracy and efficiency, we employed the Monte Carlo method to simulate the results of the one- and two-dimensional stochastic NLS equations for different sample sizes. The proposed method outperformed the Monte Carlo method in terms of calculation accuracy and efficiency. In addition, we utilized the proposed method to calculate the expectation amplitude at a specific time for the Ginzburg–Landau equation. In future work, we plan to extend the proposed method to establish mapping relationships for other types of multivariate random variables and perform numerical calculations for stochastic nonlinear Schrödinger equations.

Appendix

A. Tensor Product of Triple Hermite Polynomials

Hermite polynomials have a generating function [29, 35]

$$\psi(x,z) = e^{-z^2/2+xz} = \sum_{n=0}^{\infty} \frac{P_n(x)}{n!} z^n. \tag{A.1}$$

The unnormalized Hermite polynomials are as follows:

$$P_n(x) = \left.\frac{\partial^n \psi(x,z)}{\partial z^n}\right|_{z=0}. \tag{A.2}$$

Any three generating functions of Hermite polynomials are multiplied

$$\begin{aligned}\psi(x,\sigma)\psi(x,z)\psi(x,\omega) &= e^{-\sigma^2/2+x\sigma} e^{-z^2/2+xz} e^{-\omega^2/2+x\omega} \\ &= e^{z\omega+z\sigma+\sigma\omega} e^{x^2/2-[(z+\omega+\sigma)-x]^2/2}.\end{aligned} \tag{A.3}$$

Expanding (A.3) into a Taylor series of variable z, ω, and σ, we have

$$\begin{aligned}\psi(x,\sigma)\psi(x,z)\psi(x,\omega) &= \sum_{p=0}^{\infty} \frac{(z\omega)^p}{p!} \sum_{q=0}^{\infty} \frac{(\sigma z)^q}{q!} \sum_{r=0}^{\infty} \frac{(\sigma\omega)^r}{r!} \sum_{k=0}^{\infty} \frac{P_k(x)}{k!} (z+\sigma+\omega)^k \\ &= \sum_{p=0}^{\infty}\sum_{q=0}^{\infty}\sum_{r=0}^{\infty}\sum_{k=0}^{\infty}\sum_{m=0}^{k}\sum_{n=0}^{k-m} \frac{P_k(x)}{p!q!r!k!} \binom{k}{m}\binom{k-m}{n} \sigma^{p+r+k-m-n} \omega^{q+r+n} z^{m+p+q}, \\ &\text{Let } \nu = k-m-n \\ &= \sum_{p=0}^{\infty}\sum_{q=0}^{\infty}\sum_{r=0}^{\infty}\sum_{m=0}^{k}\sum_{n=0}^{k-m}\sum_{\nu=0}^{k-m-n} \frac{P_{m+n+\nu}(x)}{p!q!r!m!n!\nu!} z^{m+p+q} \omega^{q+r+n} \sigma^{p+r+\nu}.\end{aligned} \tag{A.4}$$

Let $\alpha = m+p+q$, $\beta = q+r+n$, and $\gamma = p+r+\nu$. Then, (A.4) can be rewritten as follows:

$$\psi(x,\sigma)\psi(x,z)\psi(x,\omega) = \sum_{\alpha=0}^{\infty}\sum_{\beta=0}^{\infty}\sum_{\gamma=0}^{\infty} \left(\sum_{p\le\alpha\wedge\gamma} \sum_{q\le\alpha\wedge\beta} \sum_{r\le\beta\wedge\gamma} \frac{P_{\alpha+\beta+\gamma-2(p+q+r)}(x)}{p!q!r!(\alpha-p-q)!(\beta-q-r)!(\gamma-p-r)!} \right) z^\alpha \omega^\beta \sigma^\gamma. \tag{A.5}$$

Considering (A.1), (A.3), and (A.5), we have

$$\frac{P_\alpha(x)}{\alpha!}\frac{P_\beta(x)}{\beta!}\frac{P_\gamma(x)}{\gamma!}=\sum_{p\le\alpha\wedge\gamma}\sum_{q\le\alpha\wedge\beta}\sum_{r\le\beta\wedge\gamma}\frac{P_{\alpha+\beta+\gamma-2(p+q+r)}(x)}{p!q!r!(\alpha-p-q)!(\beta-q-r)!(\gamma-p-r)!}. \tag{A.6}$$

Therefore,

$$P_\alpha(x)P_\beta(x)P_\gamma(x)=\sum_{p\le\alpha\wedge\gamma}\sum_{q\le\alpha\wedge\beta}\sum_{r\le\beta\wedge\gamma}\frac{\alpha!\beta!\gamma!}{p!q!r!(\alpha-p-q)!(\beta-q-r)!(\gamma-p-r)!}P_{\alpha+\beta+\gamma-2(p+q+r)}(x). \tag{A.7}$$

Consider the relationship between unnormalized Hermite polynomials and standard Hermite polynomials,

$$H_\alpha(x)H_\beta(x)H_\gamma(x)=\sum_{p\le\alpha\wedge\gamma}\sum_{q\le\alpha\wedge\beta}\sum_{r\le\beta\wedge\gamma}\frac{\sqrt{\alpha!\beta!\gamma!}\sqrt{\alpha+\beta+\gamma-2(p+q+r)}}{p!q!r!(\alpha-p-q)!(\beta-q-r)!(\gamma-p-r)!}H_{\alpha+\beta+\gamma-2(p+q+r)}(x). \tag{A.8}$$

Denote

$$\begin{aligned}B_2(\alpha,\beta,\gamma,p,q,r)&=\frac{\sqrt{\alpha!\beta!\gamma!}\sqrt{\alpha+\beta+\gamma-2(p+q+r)}}{p!q!r!(\alpha-p-q)!(\beta-q-r)!(\gamma-p-r)!}\\&=\left[\binom{\alpha}{p,q}\binom{\beta}{q,r}\binom{\gamma}{p,r}\binom{\alpha+\beta+\gamma-2(p+q+r)}{\alpha-p-q,\beta-q-r}\right]^{1/2},\\H_\alpha(x)H_\beta(x)H_\gamma(x)&=\sum_{p\le\alpha\wedge\gamma}\sum_{q\le\alpha\wedge\beta}\sum_{r\le\beta\wedge\gamma}B_2(\alpha,\beta,\gamma,p,q,r)H_{\alpha+\beta+\gamma-2(p+q+r)}(x),\end{aligned} \tag{A.9}$$

which completes the proof.

B. Tensor Product of Triple Random Functions

Suppose random functions u, v, and w have the following SG chaos expansions [29]:

$$\begin{aligned}u&=\sum_\alpha u_\alpha\phi_\alpha(\eta),\\v&=\sum_\beta v_\beta\phi_\beta(\eta),\\w&=\sum_\gamma w_\gamma\phi_\gamma(\eta),\end{aligned} \tag{B.1}$$

where α, β, and γ are any nonnegative integers, η is a one-dimensional Gaussian variable. Denote $p\le\alpha\wedge\gamma, q\le\alpha\wedge\beta, r\le\beta\wedge\gamma$.

$$uvw=\sum_{\alpha\in\mathcal{J}}\sum_{\beta\in\mathcal{J}}\sum_{\gamma\in\mathcal{J}}u_\alpha v_\beta w_\gamma\phi_\alpha(\eta)\phi_\beta(\eta)\phi_\gamma(\eta)=\sum_{\alpha\in\mathcal{J}}\sum_{\beta\in\mathcal{J}}\sum_{\gamma\in\mathcal{J}}u_\alpha v_\beta w_\gamma\sum_{p\le\alpha\wedge\gamma}\sum_{q\le\alpha\wedge\beta}\sum_{r\le\beta\wedge\gamma}B_2(\alpha,\beta,\gamma,p,q,r)\phi_{\alpha+\beta+\gamma-2(p+q+r)}(\eta). \tag{B.2}$$

Denote $\tilde{\alpha}=\alpha-p-q$, $\tilde{\beta}=\beta-q-r$, and $\tilde{\gamma}=\gamma-p-r$. Then, (B.2) can be rewritten as follows:

$$(B.2) = \sum_{\widetilde{\alpha}\in\mathcal{J}}\sum_{\widetilde{\beta}\in\mathcal{J}}\sum_{\widetilde{\gamma}\in\mathcal{J}} u_{\widetilde{\alpha}+p+q} v_{\widetilde{\beta}+q+r} w_{\widetilde{\gamma}+p+r} \times \sum_{p}\sum_{q}\sum_{r} \frac{\sqrt{(\widetilde{\alpha}+p+q)!\,(\widetilde{\beta}+q+r)!\,(\widetilde{\gamma}+p+r)!\,(\widetilde{\alpha}+\widetilde{\beta}+\widetilde{\gamma})!}}{p!q!r!\widetilde{\alpha}!\widetilde{\beta}!\widetilde{\gamma}!} \phi_{\widetilde{\alpha}+\widetilde{\beta}+\widetilde{\gamma}}(\eta). \tag{B.3}$$

For simplicity, we denote $\widetilde{\alpha} = \alpha$, $\widetilde{\beta} = \beta$, $\widetilde{\gamma} = \gamma$, and $\theta = \alpha + \beta + \gamma$. Then, (B.3) is equivalent to

$$\begin{aligned}(B.3) &= \sum_{\theta}\sum_{\theta=\widetilde{\alpha}+\widetilde{\beta}+\widetilde{\gamma}} u_{\alpha+p+q} v_{\beta+q+r} w_{\gamma+p+r} \sum_{p}\sum_{q}\sum_{r} \frac{\sqrt{(\alpha+p+q)!\,(\beta+q+r)!\,(\gamma+p+r)!\theta!}}{p!q!r!\alpha!\beta!\gamma!} \phi_{\theta}(\eta) \\ &= \sum_{\theta}\left(\sum_{p}\sum_{q}\sum_{r}\sum_{\theta=\alpha+\beta+\gamma} C_2(\theta,p,q,r,\alpha,\beta,\gamma) u_{\alpha+p+q} v_{\beta+q+r} w_{\gamma+p+r}\right)\phi_{\theta}(\eta), \\ C_2(\theta,p,q,r,\alpha,\beta,\gamma) &= \frac{\sqrt{(\alpha+p+q)!\,(\beta+q+r)!\,(\gamma+p+r)!\theta!}}{p!q!r!\alpha!\beta!\gamma!} \\ &= \left[\binom{\theta}{\alpha,\beta}\binom{\alpha+p+q}{p,q}\binom{\beta+q+r}{q,r}\binom{\gamma+p+r}{p,r}\right]^{1/2},\end{aligned} \tag{B.4}$$

which completes the proof.

Data Availability

No data were used to support the study in this article.

Conflicts of Interest

The author declares that there are no conflicts of interest.

References

[1] M. J. Ablowitz, M. Ablowitz, P. Clarkson, and P. A. Clarkson, *Solitons, Nonlinear Evolution Equations and Inverse Scattering*, vol. 149, Cambridge University Press, Cambridge, UK, 1991.

[2] V. Barbu, M. Röckner, and D. Zhang, "Stochastic nonlinear Schrödinger equations," *Nonlinear Analysis: Theory, Methods and Applications*, vol. 136, pp. 168–194, 2016.

[3] D. Chakraborty, J.-H. Jung, and E. Lorin, "An efficient determination of critical parameters of nonlinear Schrödinger equation with a point-like potential using generalized polynomial chaos methods," *Applied Numerical Mathematics*, vol. 72, pp. 115–130, 2013.

[4] A. Al-Harbi, W. Al-Hamdan, and L. Wazzan, "Numerical methods for solving logarithmic nonlinear Schrodinger's equation," *Journal of Applied Mathematics and Physics*, vol. 10, no. 12, pp. 3635–3648, 2022.

[5] J. Cui and L. Sun, "Stochastic logarithmic schrödinger equations: energy regularized approach," 2021, https://arxiv.org/abs/2102.12607.

[6] X. Feng and S. Ma, "Stable numerical methods for a stochastic nonlinear Schrödinger equation with linear multiplicative noise," *Discrete and Continuous Dynamical Systems-S*, vol. 15, p. 687, 2022.

[7] A. H. Sheinfux, E. Schleifer, J. Papeer, G. Fibich, B. Ilan, and A. Zigler, "Measuring the stability of polarization orientation in high intensity laser filaments in air," *Applied Physics Letters*, vol. 101, no. 20, 2012.

[8] J. Cui, S. Liu, and H. Zhou, "Wasserstein Hamiltonian flow with common noise on graph," *SIAM Journal on Applied Mathematics*, vol. 83, no. 2, pp. 484–509, 2023.

[9] J. Cui, J. Hong, Z. Liu, and W. Zhou, "Stochastic symplectic and multi-symplectic methods for nonlinear Schrödinger equation with white noise dispersion," *Journal of Computational Physics*, vol. 342, pp. 267–285, 2017.

[10] J. Cui, S. Liu, and H. Zhou, "Optimal control for stochastic nonlinear schrödinger equation on graph," 2022, https://arxiv.org/abs/2209.05346.

[11] J. Cui, J. Hong, Z. Liu, and W. Zhou, "Strong convergence rate of splitting schemes for stochastic nonlinear Schrödinger equations," *Journal of Differential Equations*, vol. 266, no. 9, pp. 5625–5663, 2019.

[12] J. Cui and J. Hong, "Analysis of a splitting scheme for damped stochastic nonlinear Schrödinger equation with multiplicative noise," *SIAM Journal on Numerical Analysis*, vol. 56, no. 4, pp. 2045–2069, 2018.

[13] J. Bäck, F. Nobile, L. Tamellini, and R. Tempone, "Stochastic spectral galerkin and collocation methods for pdes with random coefficients: a numerical comparison," in *Spectral and High Order Methods for Partial Differential Equations*, pp. 43–62, Springer, Berlin, Germany, 2011.

[14] J. D. Jakeman, F. Franzelin, A. Narayan, M. Eldred, and D. Plfüger, "Polynomial chaos expansions for dependent random variables," *Computer Methods in Applied Mechanics and Engineering*, vol. 351, pp. 643–666, 2019.

[15] P.-L. Liu and A. Der Kiureghian, "Multivariate distribution models with prescribed marginals and covariances," *Probabilistic Engineering Mechanics*, vol. 1, no. 2, pp. 105–112, 1986.

[16] M. Rosenblatt, "Remarks on a multivariate transformation," *The Annals of Mathematical Statistics*, vol. 23, no. 3, pp. 470–472, 1952.

[17] X. Chen, E.-J. Park, and D. Xiu, "A flexible numerical approach for quantification of epistemic uncertainty," *Journal of Computational Physics*, vol. 240, pp. 211–224, 2013.

[18] J. Jakeman, M. Eldred, and D. Xiu, "Numerical approach for quantification of epistemic uncertainty," *Journal of Computational Physics*, vol. 229, no. 12, pp. 4648–4663, 2010.

[19] D. Xiu and G. E. Karniadakis, "The wiener-askey polynomial chaos for stochastic differential equations," *SIAM Journal on Scientific Computing*, vol. 24, no. 2, pp. 619–644, 2002.

[20] S. Rahman, "Wiener-hermite polynomial expansion for multivariate Gaussian probability measures," *Journal of Mathematical Analysis and Applications*, vol. 454, no. 1, pp. 303–334, 2017.

[21] S. Rahman, "A polynomial chaos expansion in dependent random variables," *Journal of Mathematical Analysis and Applications*, vol. 464, no. 1, pp. 749–775, 2018.

[22] M. Chevreuil, R. Lebrun, A. Nouy, and P. Rai, "A least-squares method for sparse low rank approximation of multivariate functions," *SIAM/ASA Journal on Uncertainty Quantification*, vol. 3, no. 1, pp. 897–921, 2015.

[23] A. Doostan and H. Owhadi, "A non-adapted sparse approximation of pdes with stochastic inputs," *Journal of Computational Physics*, vol. 230, no. 8, pp. 3015–3034, 2011.

[24] J. D. Jakeman, M. S. Eldred, and K. Sargsyan, "Enhancing l1-minimization estimates of polynomial chaos expansions using basis selection," *Journal of Computational Physics*, vol. 289, pp. 18–34, 2015.

[25] M. Navarro, J. Witteveen, and J. Blom, "Polynomial chaos expansion for general multivariate distributions with correlated variables," 2014, https://arxiv.org/abs/1406.5483.

[26] T. Tang and T. Zhou, "On discrete least-squares projection in unbounded domain with random evaluations and its application to parametric uncertainty quantification," *SIAM Journal on Scientific Computing*, vol. 36, no. 5, pp. A2272–A2295, 2014.

[27] J. A. Witteveen and H. Bijl, "Modeling arbitrary uncertainties using gram-schmidt polynomial chaos," in *Proceedings of the 44th AIAA Aerospace sciences meeting and exhibit*, p. 896, Montreal, Canada, August, 2006.

[28] L. Yan, L. Guo, and D. Xiu, "Stochastic collocation algorithms using l1-minimization," *International Journal for Uncertainty Quantification*, vol. 2, pp. 279–293, 2012.

[29] W. Luo, *Wiener chaos expansion and numerical solutions of stochastic partial differential equations*, PHD thesis, California Institute of Technology, Pasadena, CA, USA, 2006.

[30] D. Xiu, *Numerical Methods for Stochastic Computations*, Princeton university press, Princeton, NJ, USA, 2010.

[31] H. Xie, "An efficient and spectral accurate numerical method for computing SDE driven by multivariate Gaussian variables," *AIP Advances*, vol. 12, p. 7, 2022.

[32] D. Gottlieb and D. Xiu, "Galerkin method for wave equations with uncertain coefficients," *Communications in Computational Physics*, vol. 3, no. 2, pp. 505–518, 2008.

[33] R. Cheng, L. Wu, C. Pang, and H. Wang, "A fourier collocation method for Schrödinger-Poisson system with perfectly matched layer," *Communications in Mathematical Sciences*, vol. 20, no. 2, pp. 523–542, 2022.

[34] J. Shen, T. Tang, and L.-L. Wang, *Spectral Methods: Algorithms,Analysis and Applications*, vol. 41, Springer Science &Business Media, Berlin, Germany, 2011.

[35] R. Courant and D. Hilbert, *Methods of Mathematical Physics: Partial Differential Equations*, John Wiley &Sons, Hoboken, NJ, USA, 2008.